Desalination and Water Treatment
www.deswater.com
doi: 10.1080/19443994.2015.1067925

57 (2016) 14986–14996
July

Taylor & Francis
Taylor & Francis Group

Preparation of hydrazine-modified CMC/Fe_3O_4 hybrid magnetic particles for adsorption of Reactive Blue 21 from water

Peng Wang, Tingguo Yan, Qianyun Ma, Dongying Hu, Lijuan Wang*

Key Laboratory of Bio-based Materials Science and Technology of Ministry of Education, Northeast Forestry University, 26 Hexing Road, Harbin, P.R. China, Tel. +86 18745068285; email: wangpeng8917@126.com (P. Wang), Tel. +86 18246196553; email: tingguoyan@126.com (T. Yan), Tel. +86 13091883562; email: maqianyun@126.com (Q. Ma), Tel. +86 15045017413; email: sigl1234@163.com (D. Hu), Tel./Fax: +86 451 82191693; email: donglinwlj@163.com (L. Wang)

Received 28 January 2015; Accepted 26 June 2015

ABSTRACT

In this work, chemically modified carboxymethyl cellulose/Fe_3O_4 particles (MCMC/Fe_3O_4) with hydrazine were prepared and characterized by scanning electron microscopy, X-ray diffraction, and vibrating sample magnetometer. Batch adsorption experiments were performed to remove Reactive Blue 21 (RB 21) from aqueous solution. Various parameters such as pH, initial dye concentration, adsorbent dosage, contact time, and temperature had been studied. Kinetic studies showed that the dye adsorption process followed a pseudo-second-order kinetic model. The equilibrium data were well described by Langmuir and Dubinin–Radushkevich model. Furthermore, the thermodynamic parameters (positive values of ΔH° and ΔS°, negative values of ΔG°) revealed the feasibility, spontaneity, and endothermic nature of the adsorption.

Keywords: Adsorption; Fe_3O_4; Carboxymethyl cellulose (CMC); Kinetics; Mechanism

1. Introduction

Dyes are widely used in many industries such as textile, cosmetics, paper printing, leather, and plastic industry [1]. These dyes are difficult to degrade because of their complex aromatic structures and can cause allergy, dermatitis, irritation, and even to cancer in humans [2]. Therefore, removal of dyes is essential procedure of wastewater treatment before discharge [3]. Various methods including adsorption, chemical precipitation, ion exchange, coagulation, electrolysis, and membrane process have been developed to remove dyes from wastewater [4–7]. Among them, adsorption is considered to be one of the simplest and most attractive methods for dealing with wastewater [8]. A commonly used adsorbent, activated carbon has been widely investigated and used for dye adsorption from various effluents. Nevertheless, its application is limited because of its high cost and recalcitrant [9]. Hence, in the past few years, biosorbents prepared from nature organisms are paid much more attentions. These sorbents, such as starch, cellulose, chitosan, and lignin, are easily biodegradable and nontoxic. Nowadays, there are a number of articles reporting the adsorptive removal of dye by these biosorbents [10–18].

Cellulose is one of the most abundant natural polymers with excellent biodegradability and biocompatibility. However, the compact and inactive molecular structure of cellulose requires it to be modified to

*Corresponding author.

improve its hydrophilicity as an adsorbent for dye removal [19]. Currently, the most widely adopted methods for modification of cellulose include esterification, etherification, halogenation, and oxidation [20–23]. Sodium carboxymethyl cellulose (CMC) is a representative cellulose derivative with carboxymethyl groups (–CH_2COONa) bound to some of the hydroxyl groups on the cellulose backbone. The polar carboxyl groups render the cellulose soluble, chemically reactive, and strongly chelate; therefore, the application of CMC in adsorption fields becomes attractive and promising [24–28]. Hydrazine is a kind of important derivatizing agents. It has been reported that hydrazine on the surface of cellulose or lignin can favor metal ion adsorption through the chelation mechanism [29,30]. However, it is difficult to separate adsorbents from the solution rapidly after the adsorption using traditional separation methods such as filtration and sedimentation. Recently, magnetic separation technology is paid growing attention [31–33]. Magnetic materials can be quickly separated from the water and effectively controlled by applying a magnetic field [34].

In this work, we prepared magnetic CMC/Fe_3O_4 particles modified with hydrazine as an adsorbent to remove RB 21 from aqueous solution. The morphology, structure, and magnetic properties of magnetic particles were characterized by scanning electron microscopy (SEM), X-ray diffraction (XRD), and vibrating sample magnetometer (VSM). The adsorption of RB 21 onto MCMC/Fe_3O_4 particles was tested under various conditions. Kinetic, isotherm, and thermodynamics parameters were also investigated.

2. Materials and methods

2.1. Materials

CMC (DS = 0.92, Chemical pure, 300–800 mPa s (20 g L^{-1}, 25°C)) is purchased from Sinopharm Chemical Reagent Co., Ltd, China. The $FeCl_3{\cdot}6H_2O$, $FeSO_4{\cdot}7H_2O$, NaOH, $NaIO_4$, and CH_3COOH used were of analytical grade and purchased from Tianjin Kermel Chemical Reagent Co., Ltd, China. Reactive Blue 21 (RB 21) was obtained commercially from Shanghai Dystar Trade Co., Ltd. All chemicals were used without further purification. Distilled water was used in all the experiments.

2.2. Preparation of adsorbent

One gram of CMC was dissolved in 20 mL distilled water. After complete dissolution, 10 mL (0.11 g L^{-1}) sodium periodate solution was added and the pH of the solution was adjusted to 3.0 with 2 mol L^{-1} sulfuric acid. And then, the mixture was stirred vigorously at 35°C for 4 h. Finally, the products were washed with distilled water and ethanol and then dried in an oven at 60°C overnight for further use.

$FeCl_3{\cdot}6H_2O$ (7.0047 g) and $FeSO_4{\cdot}7H_2O$ (4.1169 g) were dissolved in 200 mL of prepared CMC solution, and the solution was stirred vigorously under a nitrogen atmosphere at 55°C for 30 min. Chemical precipitation was executed by the slow addition of NaOH solution (2 mol L^{-1}) to adjust the pH value to 9–10. After 90 min, precipitated products were magnetically separated and washed with distilled water and ethanol and dried in a vacuum oven at 60°C.

As-prepared CMC/Fe_3O_4 particles were dispersed in 750 mL acetated buffer (pH 4.5) and 15 mL hydrazine solution was added under mechanical stirring at room temperature for 24 h. Finally, the modified CMC/Fe_3O_4 particles were washed several times with distilled water and ethanol and then dried at 60°C. Fig. 1 shows the preparation sketch of MCMC/Fe_3O_4.

2.3. Characterization of MCMC/Fe_3O_4

The surface morphologies of the products were characterized using SEM (Quanta 200) with an accelerating voltage of 15 kV. The crystal structures of the particles were determined by X-ray diffraction (XRD, Rigaku D/max-2200 diffractometer) using Cu Kα radiation at 40 kV and 30 mA. Magnetic hysteresis loops were obtained at 300 K using a VSM.

2.4. Adsorption experimental

Standard solutions of different concentrations were prepared by diluting the 1,000 mg L^{-1} RB 21 stock solution. The adsorption of RB 21 from standard solution was performed using batch technique in a thermostatic shaker bath at 120 rpm. After adsorption, the adsorbent was removed from the solution using an adscititious magnet. The concentration of the residual RB 21 was analyzed using a UV–vis spectrophotometer. The amount of dyes adsorbed on the bioadsorbent, q_t (mg g^{-1}), was calculated with the following equation:

$$q_t = \frac{(C_0 - C_t)V}{W} \quad (1)$$

where C_0 and C_t are the initial dye concentration (mg L^{-1}) and instantaneous dye concentration (mg L^{-1}), respectively, V is the volume of the dye solution (L), and W is the weight of the adsorbent (g).

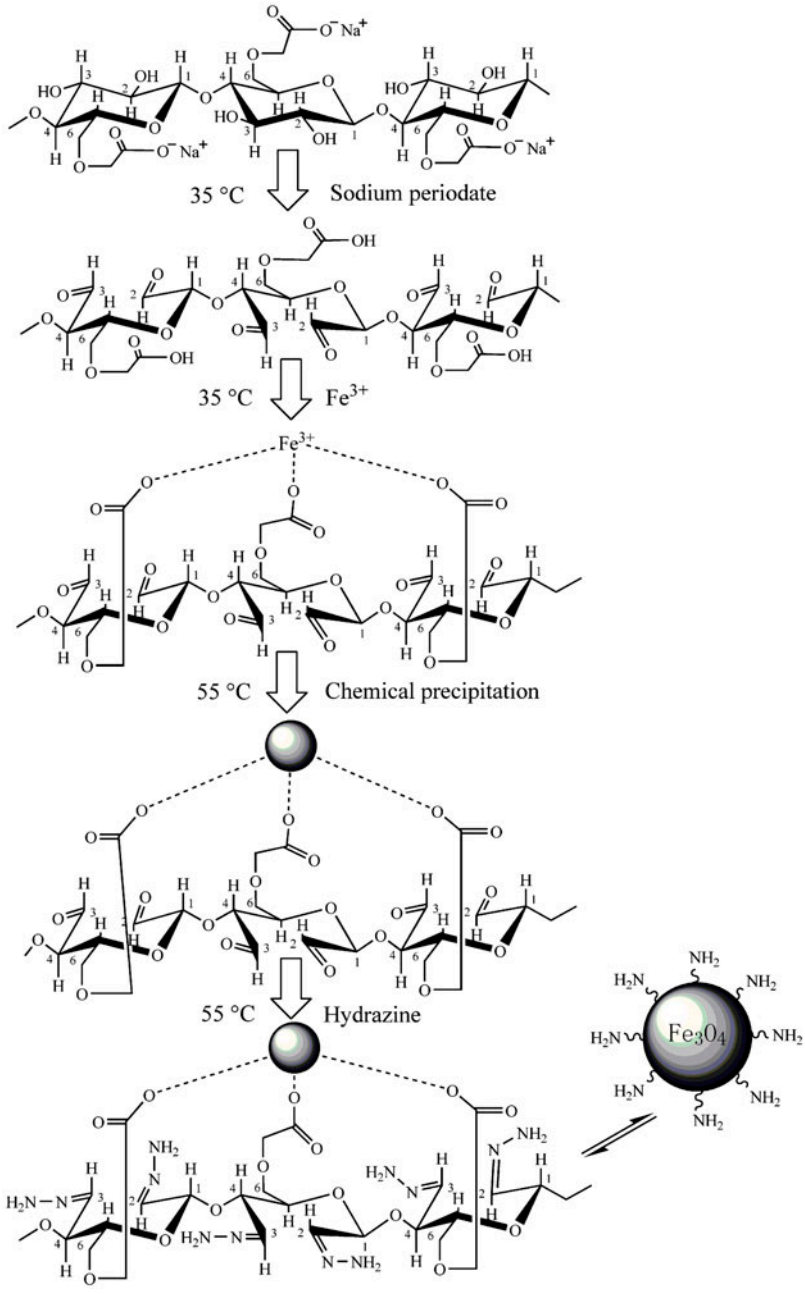

Fig. 1. Scheme for the preparation of MCMC/Fe_3O_4.

3. Results and discussion

3.1. Characterization of adsorbent

3.1.1. SEM analysis

SEM photographs of the Fe_3O_4 and MCMC/Fe_3O_4 particles are shown in Fig. 2. From Fig. 2(a), it is clear that the naked Fe_3O_4 particles were almost spherical with diameters range from 1 to 3 μm. Most of the particles were physically aggregated due to strong magnetic magneto-dipole attractions between particles. For the MCMC/Fe_3O_4 samples, the surface morphology showed little change, but the size of the particles became smaller since the electrostatic interaction between the Fe_3O_4 particles and CMC in the coating process increased the repulsive force of the magnetic particles.

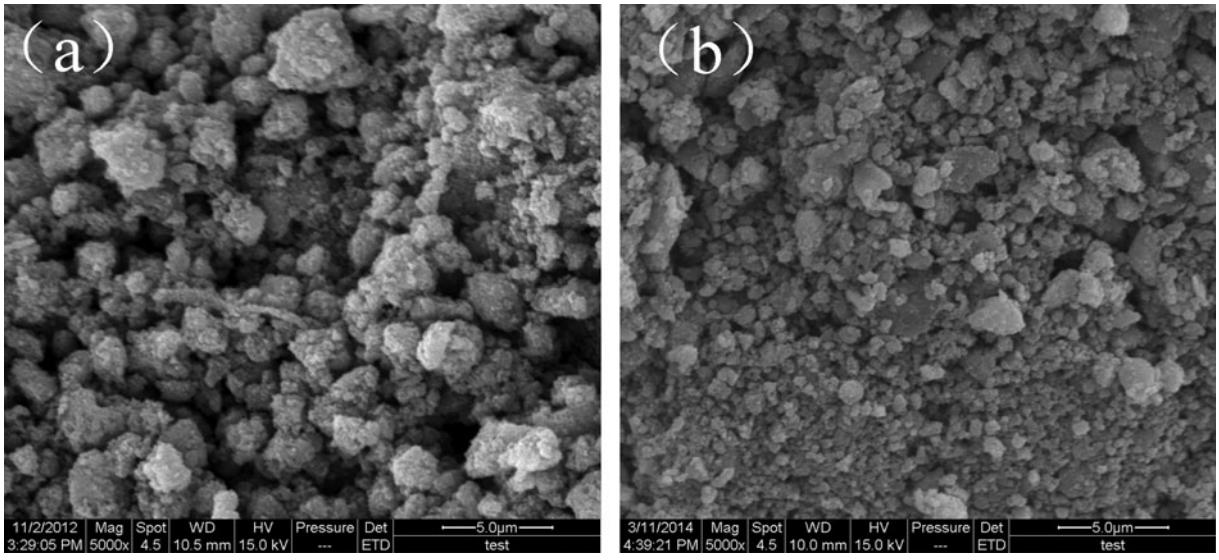

Fig. 2. SEM photographs of the Fe_3O_4 (a) and MCMC/Fe_3O_4 (b) particles.

3.1.2. XRD analysis

XRD patterns of pure Fe_3O_4 (a) and MCMC/Fe_3O_4 (b) are shown in Fig. 3. Six characteristic peaks for Fe_3O_4 ($2\theta = 30.72$, 35.38, 43.72, 53.64, 57.24, and 62.86°) marked by their indices (2 2 0), (3 1 1), (4 0 0), (4 2 2), (5 1 1), and (4 4 0) were observed for both samples. These peaks are consistent with the database JCPDS file (PDF No. 79-0418) and reveals that the resultant particles are pure Fe_3O_4 with a spinel structure [35]. It is also explained that the CMC-coating process and the hydrazine functionalization process did not result in Fe_3O_4 particle phase change [36].

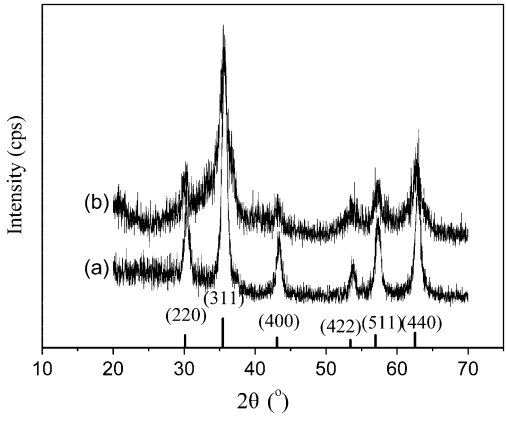

Fig. 3. XRD patterns of the pure Fe_3O_4 (a) and MCMC/Fe_3O_4 (b) particles.

3.1.3. Magnetic properties

Fig. 4 shows the hysteresis loop of Fe_3O_4 (a) and MCMC/Fe_3O_4 (b) at 300 K. The saturation magnetization of MCMC/Fe_3O_4 was ~28.57 emu g^{-1}, which is lower than those of pure Fe_3O_4 (70.08 emu g^{-1}) [37]. No remanence and coercivity were observed, which indicates that Fe_3O_4 and MCMC/Fe_3O_4 were superparamagnetic. It can also be seen that the magnetic particles dispersed well in water and aggregated within 1 min when a magnet was nearby. The results illustrated that the magnetic property of this adsorbent

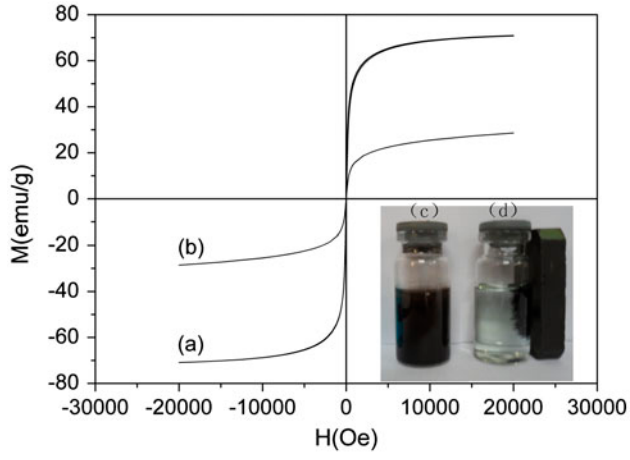

Fig. 4. Magnetic hysteresis curves of Fe_3O_4 (a) and MCMC/Fe_3O_4 (b) at 300 K and photographs of MCMC/Fe_3O_4 suspended in water in the absence (c) and in the presence (d) of an externally placed magnet.

could ensure a feasible application in liquid separation systems.

3.2. Effect of initial pH on adsorption

The solution pH is one of the dominant parameters affecting the adsorption process. The effect of initial pH on RB 21 adsorption is shown in Fig. 5. It was found that the removal efficiency decreased from 94.47 to 40.04% with the increase in pH from 1.08 to 10.00. This may be related to the electrostatic attraction between anionic dye and adsorbent. In weakly solution, more protons were available to protonate amine group to form $-NH_3^+$ group with positive charge, which resulted in enhancing the electrostatic attraction between negatively charge dye anions and positively charge surface of MCMC/Fe_3O_4. As the pH increased, the number of positively charge active sites decreased and the presence of excess OH^- ions destabilizing anionic dye and competing with the dye anions for adsorption sites. Therefore, lower removal percentages were observed at alkaline pH values for RB 21 adsorption.

3.3. Effect of contact time and initial temperature

The effects of contact time and temperature on the adsorption of RB 21 onto MCMC/Fe_3O_4 are shown in Fig. 6. The adsorption capacity rapidly increased at initial stage of the adsorption process and completely reached equilibrium after 240 min. This may be due to the fact that there are abundant vacant surface sites available for adsorption during the initial stage, and hence, the extent of removal is high. The adsorption capacity at equilibrium was found to increase from 60.32 to 72.59 mg g^{-1} for an increase in temperature from 30 to 60°C. It was clear that higher temperature favored adsorption of RB 21 onto MCMC/Fe_3O_4 particles.

3.4. Effect of adsorbent dose and initial concentration

The effect of adsorbent dose on adsorption of RB 21 is shown in Fig. 7(a). The adsorption capacity decreased from 101.84 to 31.10 mg g^{-1} with increasing adsorbent dose from 20 to 80 mg. This resulted from the split in the flux or the concentration gradient of the dye between the aqueous and solid phase [38]. However, the percentage dye removal increased from 83.51 to 99.90% as the adsorbent dose increased from 20 to 80 mg. This result is expected because of the increase in sorption active sites at the adsorbent surface with increasing dose [39].

The effect of initial RB 21 concentration on the percentage removal of the dye is shown in Fig. 7(b). The removal rate increased from 76.37 to 99.69% when the initial concentration was increased from 40 to 100 mg L^{-1}. This is due to increase in the driving force of the concentration gradient, as an increase in the initial dye concentration.

3.5. Adsorption kinetics

To investigate the adsorption mechanism and its potential rate-controlling steps, the pseudo-first-order, pseudo-second-order, intraparticle diffusion, and Boyd's film-diffusion kinetic models were used to test the experimental data.

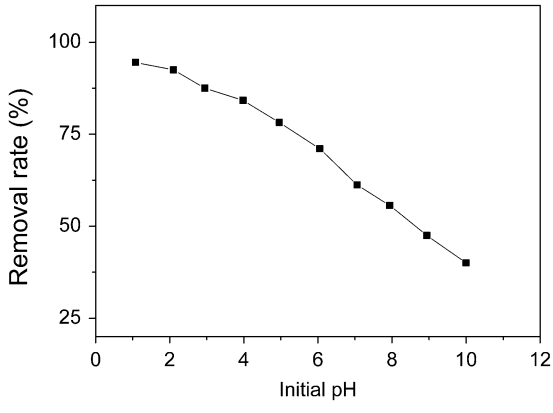

Fig. 5. Effect of initial solution pH on the adsorption of RB 21 onto MCMC/Fe_3O_4 (C = 50 mg L^{-1}, V = 50 mL, T = 30°C, t = 720 min, and dosage = 20 mg).

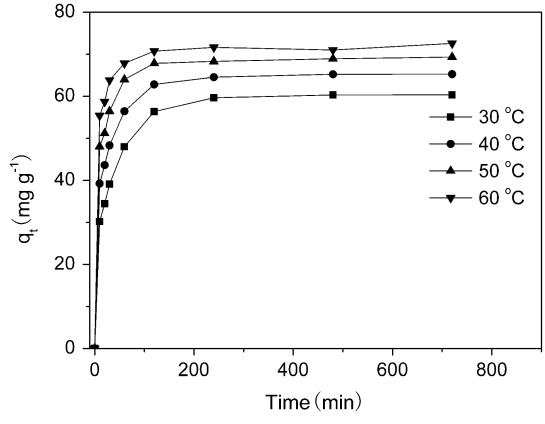

Fig. 6. Effect of contact time and temperature on the adsorption of RB 21 onto MCMC/Fe_3O_4 (C = 50 mg L^{-1}, V = 50 mL, and dosage = 20 mg).

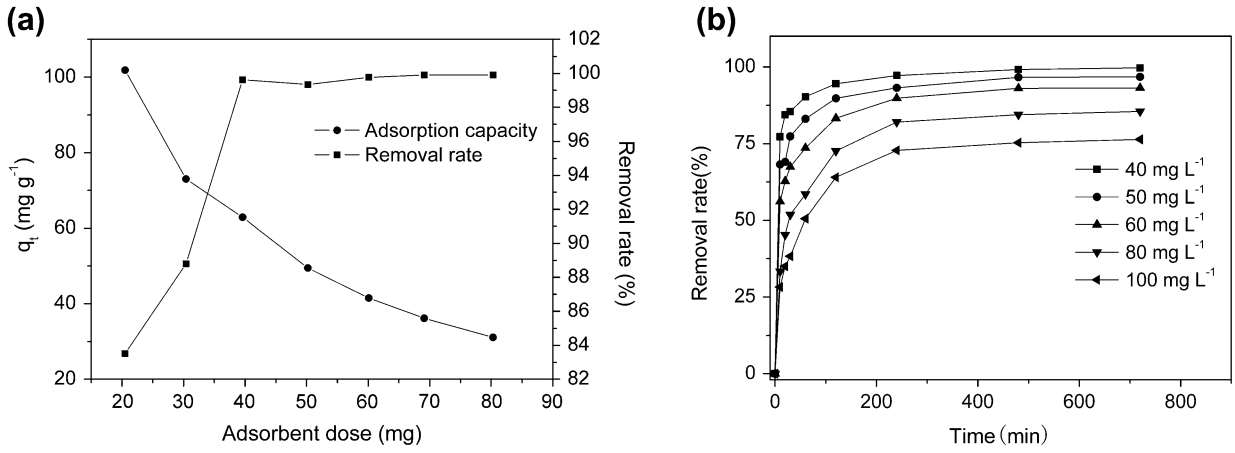

Fig. 7. Effect of adsorbent dose (a) (C = 50 mg L^{-1}, V = 50 mL, T = 30°C, and t = 720 min) and initial dye concentration and (b) (V = 50 mL, T = 30°C, and dosage = 20 mg) on the adsorption of RB 21 onto MCMC/Fe_3O_4.

The pseudo-first-order equation can be expressed as follows [40]:

$$q_t = q_e(1 - e^{-k_1 t}) \quad (2)$$

$$\ln\,(q_e - q_t) = \ln\, q_e - k_1 t \quad (3)$$

where q_e and q_t are the amount of RB 21 (mg g^{-1}) adsorbed on the adsorbent at equilibrium and at a given time t (min), respectively, and k_1 is the rate constant (min^{-1}) of the Lagergren-first-order kinetic model. Values of k_1 are calculated from plots of ln ($q_e - q_t$) vs. t. The pseudo-second-order kinetic model is expressed as [41]:

$$q_t = \frac{k_2 q_e^2 t}{1 + k_2 q_e t} \quad (4)$$

$$\frac{t}{q_t} = \frac{1}{k_2 q_e^2} + \frac{t}{q_e} \quad (5)$$

where k_2 is the rate constant of pseudo-second-order adsorption (g mg^{-1}min^{-1}). Values of k_2 are obtained from a plot of (t/q_t) vs. t.

The experimental data were prior analyzed by a comparison of q_t against time from these two kinetic models and subsequently determined by linear regression. The regression plots of two models are presented in Fig. 8(a) and (b), and the kinetic parameters and correlation coefficients (R^2) are summarized in Table 1. The correlation coefficient values that obtained for the pseudo-second-order kinetic model were higher than those of the first-order model. Moreover, the theoretical $q_{e,cal}$ values were also much closer to the experimental $q_{e,exp}$ values. This suggests that the pseudo-second-order kinetic model was more valid to describe the adsorption of RB 21 onto MCMC/Fe_3O_4. The rate-limiting step may therefore be a chemical sorption involving valance forces through the sharing or exchange of electrons between the adsorbent and sorbate [42].

In order to identify diffusion mechanism of adsorption process, the intraparticle diffusion model was used to analyze the adsorption kinetic data, which can be expressed as follows [43]:

$$q_t = k_{id} t^{1/2} + I \quad (6)$$

where k_{id} is the intraparticle diffusion rate constant (mg g^{-1} min$^{-1/2}$) and I is the intercept (mg g^{-1}), which can be calculated from the slop of the linear plots of q_t vs. $t^{-1/2}$ as shown in Fig. 9(a). In our case, the sorption process was comprised of two sections. The initial section indicated a boundary layer effect, whereas the second section implied intraparticle or pore diffusion. As seen in Fig. 9(a), none of the lines passed through the origin. This indicates that the intraparticle diffusion was involved in the adsorption, but was not the only rate-controlling step [44].

To determine the actual rate-controlling step of the adsorption, the obtained data were further analyzed using the Boyd's film-diffusion model given by [45]:

$$B_t = -0.4977 - \ln\,(1 - F) \quad (7)$$

$$F = \frac{q_t}{q_e} \quad (8)$$

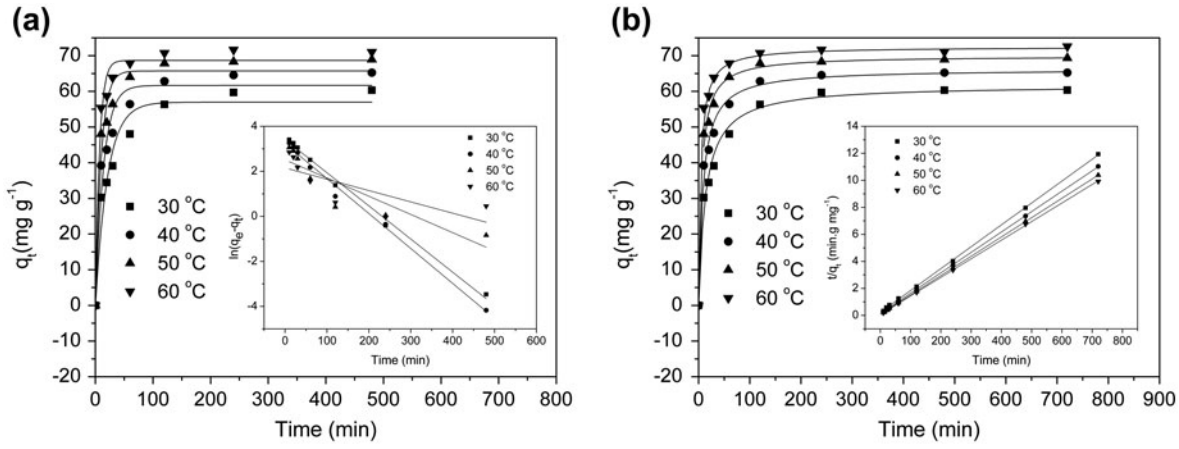

Fig. 8. Lagergren-first-order (a) and pseudo-second-order (b) kinetic model for adsorption of RB 21 onto MCMC/Fe_3O_4.

Table 1
Kinetic parameters for RB 21 adsorption onto MCMC/Fe_3O_4

T (℃)	30	40	50	60
$q_{e,exp}$ (mg g^{-1})	60.3	65.3	69.4	72.6
Pseudo-first order				
$q_{1e,cal}$ (mg g^{-1})	30.3	25.3	12.3	8.6
$k_1 \times 10^3$ (min^{-1})	14.7	15.5	8.1	5.0
R^2	0.994	0.992	0.809	0.569
Pseudo-second order				
$q_{2e,cal}$ (mg g^{-1})	61.7	66.2	69.9	72.5
$k_2 \times 10^4$ (g mg^{-1} min^{-1})	1.2	1.7	2.5	3.3
R^2	1.000	1.000	1.000	1.000
Intraparticle diffusion				
k_{id} (mg g^{-1} min$^{-1/2}$)	0.23	0.15	0.10	0.09
Intercept (mg g^{-1})	54.87	61.72	66.81	69.86
R_1^2	0.986	0.97	0.926	0.880
R_2^2	0.700	0.791	0.999	0.552
Boyd's film diffusion				
Intercept	0.08	0.24	0.46	0.87
R^2	0.998	1.000	0.994	0.975

where q_t and q_e are the adsorption capacity (mg g^{-1}) at time t and equilibrium, respectively. F is the fraction of solute adsorbed at different time t and B_t is a mathematical function of F. The calculated values were plotted against time t (min) as shown in Fig. 9(b). The Boyd parameters are listed in Table 1. The linear lines for all temperature did not pass though the origin, and the points were scattered. This suggested that the adsorption of RB 21 onto MCMC/Fe_3O_4 was mainly governed by film diffusion or external mass transport [46].

3.6. Adsorption isotherms

The equilibrium adsorption isotherm is widely used to describe the interactive behavior between the solution and the adsorbent. The equilibrium adsorption data of RB 21 on MCMC/Fe_3O_4 at different temperatures were subjected to three different adsorption isotherms, namely Langmuir, Freundlich, and Dubinin–Radushkevich (D–R) isotherms. The linearized Langmuir and Freundlich isotherm equation can be expressed as follows:

$$\frac{C_e}{q_e} = \frac{C_e}{q_{max}} + \frac{1}{q_{max} K_L} \tag{9}$$

$$\ln q_e = \ln K_F + \frac{1}{n} C_e \tag{10}$$

where q_e is the adsorbed value of RB 21 at an equilibrium concentration (mg g^{-1}), C_e is the equilibrium concentration (mg L^{-1}), q_{max} is the maximum adsorption capacity (mg g^{-1}), and K_L is the Langmuir adsorption constant, which is related to the energy of adsorption (L mg^{-1}). n is the heterogeneity factor and K_F is the Freundlich constant (L mg^{-1}). The linearized forms of two isotherm models are presented in Fig. 10, and the theoretical parameters along with regression coefficients (R^2) are listed in Table 2. As indicated by the correlation coefficients R^2, the adsorption processes were better described by the Langmuir isotherm model, which indicates that the adsorption process is mainly monolayer. The values of n are larger than 1, which indicates the favorable nature of the adsorption.

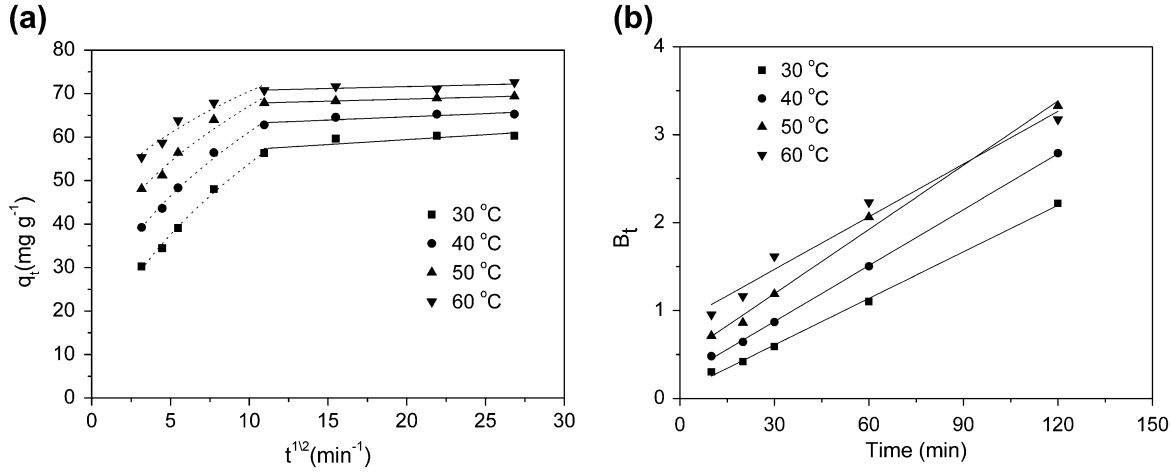

Fig. 9. The plots of intra-particle diffusion (a) and Boyd's film-diffusion (b) kinetic model for adsorption of RB 21 onto MCMC/Fe_3O_4.

Further, an essential feature of the Langmuir model can be expressed by a dimensionless constant separation factor, R_L, which is defined by the following equation [47]:

$$R_L = \frac{1}{1 + K_L C_0} \tag{11}$$

where K_L is the Langmuir equilibrium constant (L mg^{-1}) and C_0 is the initial concentration of dye (mg L^{-1}). Isotherm is considered to be unfavorable ($R_L > 1$), linear ($R_L = 1$), favorable ($1 > R_L > 0$), or irreversible ($R_L = 0$) depending on the value of R_L. In this study, all R_L values ranged from 2.78×10^{-3} to 7.85×10^{-3}, which indicates the suitability of MCMC/Fe_3O_4 for RB 21 adsorption.

The Dubinin–Radushkevich (D–R) model was used to determine the characteristic porosity and the apparent free energy of adsorption. The D–R isotherm (Fig. 10(c)) can be defined by the following equation [48]:

$$\ln q_e = \ln q_m - K\varepsilon^2 \tag{12}$$

where K is a constant related to the adsorption energy, the q_m is the D–R adsorption capacity (mg g^{-1}), and ε is the Polanyi potential calculated from Eq. (13):

$$\varepsilon = RT \ln\left(1 + \frac{1}{C_e}\right) \tag{13}$$

where C_e is the equilibrium concentration of the dye (mg L^{-1}), R is the gas constant (8.314 J K^{-1} mol^{-1}), and T is the temperature (K). The D–R constant (K) can give the valuable information regarding the mean energy of adsorption by Eq. (14):

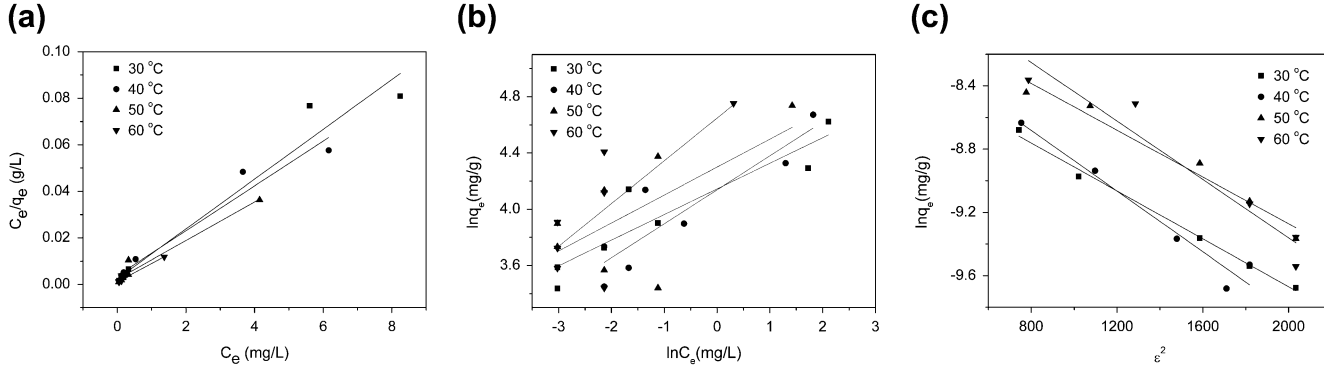

Fig. 10. Langmuir (a), Freundlich (b), and D–R (c) isotherms for the adsorption of RB 21 by MCMC/Fe_3O_4 at different temperatures.

Table 2
Langmuir, Freundlich, and D–R isotherm constants at different temperatures

	Langmuir isotherm constants				Freundlich isotherm constants			D–R isotherm constants	
T (K)	q_{max}	K_L	$R_L \times 10^3$	R^2	K_F	n	R^2	E	R^2
303	93.46	4.45	4.47	0.963	63.07	5.49	0.853	25.00	0.994
313	104.17	2.53	7.85	0.961	62.67	4.14	0.819	22.36	0.955
323	120.48	3.77	5.27	0.961	73.65	5.03	0.438	26.73	0.968
333	126.58	7.18	2.78	0.958	104.40	3.29	0.585	23.57	0.930

Table 3
Thermodynamic parameters for the adsorption of RB 21 onto MCMC/Fe_3O_4

T (K)	K_c (L mg^{-1})	ΔG° (kJ mol^{-1})	ΔH° (kJ mol^{-1})	ΔS° (J mol^{-1} K^{-1})
303	3.30	−2.25	10.44	293.91
313	5.62	−5.19		
323	13.68	−8.13		
333	79.46	−11.07		

$$E = (-2K)^{-1/2} \tag{14}$$

where E is the mean adsorption energy. The results are shown in Table 2. The mean is the transfer of free energy of one mole of solute from infinity in solution to the surface of adsorbent. The adsorption behavior could be predicted as the physical adsorption in the range of 1–8 kJ mol^{-1} and the chemical adsorption in more than 8 kJ mol^{-1} [49]. The mean adsorption energies (E) for RB 21 from 22.36 to 26.73 kJ mol^{-1} reflected that the adsorption was predominant on the chemisorption process.

3.7. Adsorption thermodynamics

The thermodynamic parameters such as Gibbs free energy change (ΔG°), enthalpy change (ΔH°), and entropy change (ΔS°) for the adsorption of RB 21 on MCMC/Fe_3O_4 have been determined using the following Van't Hoff equation [50]:

$$\Delta G^\circ = \Delta H^\circ - T\Delta S^\circ = -RT \ln K_c \tag{15}$$

$$K_c = \frac{C_s}{C_e} \tag{16}$$

$$\ln K_c = \frac{\Delta S^\circ}{R} - \frac{\Delta H^\circ}{RT} \tag{17}$$

where ΔG° (kJ mol^{-1}), ΔH° (kJ mol^{-1}), and ΔS° (J mol^{-1} K^{-1}) are changes in Gibbs free energy, enthalpy, and entropy, respectively; R is the ideal gas constant (8.314 J mol^{-1} K^{-1}); T is the absolute temperature (K); and K_c, the equilibrium constant, is the ratio of concentration of RB 21 on the adsorbent at equilibrium (C_s) to the remaining concentration of dye in solution at equilibrium (C_e). The ΔH° and ΔS° values can be calculated from the slop and intercept of the plot of ln K_c against $1/T$. The thermodynamic parameters of RB 21 are summarized in Table 3. The negative values of ΔG° imply the spontaneity and feasibility of the adsorption. The decrease in ΔG° value with increasing temperature reveals that adsorption of RB 21 onto MCMC/Fe_3O_4 becomes more favorable at higher temperature which is consistent with the results of the adsorption. The positive value of ΔH° further confirms that the adsorption process is endothermic in nature. The positive value of ΔS° suggests the increase randomness at the solid/solution interface during the adsorption of RB 21.

4. Conclusions

A new magnetic composite bioadsorbent based on Fe_3O_4 and CMC was prepared using one-step method. And then, the product was modified through the reaction with hydrazine solution to increase the contents of amino groups. SEM, X-ray diffractometry, and vibrating sample magnetometry were used to characterize the obtained magnetic adsorbent. The saturation magnetization of the magnetic adsorbent was around 28.57 emu g^{-1}, which indicated that the magnetic particles can be easily separated from aqueous

solution with an external magnetic field. Batch adsorption experiments were performed to remove anionic dye Reactive Blue 21 from aqueous solution. The results showed that the adsorption capability increased with an increase in initial dye concentration, contact time, and temperature but decreased with increase in solution pH and amount of adsorbent. The kinetic study revealed that the dye adsorption accurately followed the second-order adsorption process, while both the intraparticle diffusion and Boyd kinetic model indicated that film diffusion was the main rate determining step. The experimental isotherm data, at various temperatures, were analyzed using three isotherm models, namely Langmuir, Freundlich, and Dubinin–Radushkevich isotherm models. The results revealed that the adsorption behavior fitted well with Langmuir and Dubinin–Radushkevich isotherm. Additionally, the mean adsorption energy (E) from Dubinin–Radushkevich isotherm indicated that the adsorption process was predominant on the chemisorption. The thermodynamic parameters of free energy (ΔG°), enthalpy (ΔH°), and entropy (ΔS°) were calculated and indicated that the adsorption was feasible, spontaneous, and exothermic process in nature.

Acknowledgments

The authors gratefully acknowledge support from the Fundamental Research Funds for the Central Universities (DL12DB04).

References

[1] C. Zhou, Q. Wu, T. Lei, I.I. Negulescu, Adsorption kinetic and equilibrium studies for methylene blue dye by partially hydrolyzed polyacrylamide/cellulose nanocrystal nanocomposite hydrogels, Chem. Eng. J. 251 (2014) 17–24.

[2] M.T. Yagub, T.K. Sen, S. Afroze, H.M. Ang, Dye and its removal from aqueous solution by adsorption: A review, Adv. Colloid Interface Sci. 209 (2014) 172–184.

[3] W. Zou, S. Gao, X. Zou, H. Bai, Adsorption of neutral red and malachite green onto grapefruit peel in single and binary systems, Water Environ. Res. 85 (2013) 466–477.

[4] A.Z. Badruddoza, Z.B. Shawon, W.J. Tay, K. Hidajat, M.S. Uddin, Fe_3O_4/cyclodextrin polymer nanocomposites for selective heavy metals removal from industrial wastewater, Carbohydr. Polym. 91 (2013) 322–332.

[5] B. Shi, G. Li, D. Wang, C. Feng, H. Tang, Removal of direct dyes by coagulation: The performance of preformed polymeric aluminum species, J. Hazard. Mater. 143 (2007) 567–574.

[6] M. Amini, M. Arami, N.M. Mahmoodi, A. Akbari, Dye removal from colored textile wastewater using acrylic grafted nanomembrane, Desalination 267 (2011) 107–113.

[7] M.S. Oncel, A. Muhcu, E. Demirbas, M. Kobya, A comparative study of chemical precipitation and electrocoagulation for treatment of coal acid drainage wastewater, J. Environ. Chem. Eng. 1 (2013) 989–995.

[8] A. Srinivasan, T. Viraraghavan, Decolorization of dye wastewaters by biosorbents: A review, J. Environ. Manage. 91 (2010) 1915–1929.

[9] G. Zhang, L. Yi, H. Deng, P. Sun, Dyes adsorption using a synthetic carboxymethyl cellulose-acrylic acid adsorbent, J. Environ. Sci. 26 (2014) 1203–1211.

[10] H. Yan, W. Zhang, X. Kan, L. Dong, Z. Jiang, H. Li, H. Yang, R. Cheng, Sorption of methylene blue by carboxymethyl cellulose and reuse process in a secondary sorption, Colloids Surf., A 380 (2011) 143–151.

[11] Y.L. Zhang, J. Zhang, C.M. Dai, X.F. Zhou, S.G. Liu, Sorption of carbamazepine from water by magnetic molecularly imprinted polymers based on chitosan-Fe_3O_4, Carbohydr. Polym. 97 (2013) 809–816.

[12] D.W. O'Connell, C. Birkinshaw, T.F. O'Dwyer, Heavy metal adsorbents prepared from the modification of cellulose: A review, Bioresour. Technol. 99 (2008) 6709–6724.

[13] V.K. Gupta, Suhas, Application of low-cost adsorbents for dye removal—A review, J. Environ. Manage. 90 (2009) 2313–2342.

[14] H. Chen, X. Wang, J. Li, X. Wang, Cotton derived carbonaceous aerogels for the efficient removal of organic pollutants and heavy metal ions, J. Mater. Chem. 3 (2015) 6073–6081.

[15] H. Chen, J. Li, X. Wu, X. Wang, Synthesis of alumina-modified cigarette soot carbon as an adsorbent for efficient arsenate removal, Ind. Eng. Chem. Res. 53 (2014) 16051–16060.

[16] J. Li, S. Chen, G. Sheng, J. Hu, X. Tan, X. Wang, Effect of surfactants on Pb(II) adsorption from aqueous solutions using oxidized multiwall carbon nanotubes, Chem. Eng. J. 166 (2011) 551–558.

[17] G. Zhao, J. Li, X. Wang, Kinetic and thermodynamic study of 1-naphthol adsorption from aqueous solution to sulfonated graphene nanosheets, Chem. Eng. J. 173 (2011) 185–190.

[18] S. Zhang, M. Zeng, W. Xu, J. Li, J. Li, J. Xu, X. Wang, Polyaniline nanorods dotted on graphene oxide nanosheets as a novel super adsorbent for Cr(vi), Dalton Trans. 42 (2013) 7854–7858.

[19] X. Sun, L. Yang, Q. Li, J. Zhao, X. Li, X. Wang, H. Liu, Amino-functionalized magnetic cellulose nanocomposite as adsorbent for removal of Cr(VI): Synthesis and adsorption studies, Chem. Eng. J. 241 (2014) 175–183.

[20] J.A. Ávila Ramírez, C.J. Suriano, P. Cerrutti, M.L. Foresti, Surface esterification of cellulose nanofibers by a simple organocatalytic methodology, Carbohydr. Polym. 114 (2014) 416–423.

[21] Z. Li, D. Zhang, J. Weng, B. Chen, H. Liu, Synthesis and characterization of photochromic azobenzene cellulose ethers, Carbohydr. Polym. 99 (2014) 748–754.

[22] Y. Zhou, Q. Jin, T. Zhu, Y. Akama, Adsorption of chromium (VI) from aqueous solutions by cellulose modified with β-CD and quaternary ammonium groups, J. Hazard. Mater. 187 (2011) 303–310.

[23] L. Qiu, Z. Shao, D. Wang, F. Wang, W. Wang, J. Wang, Novel polymer Li-ion binder carboxymethyl cellulose derivative enhanced electrochemical performance for Li-ion batteries, Carbohydr. Polym. 112 (2014) 532–538.
[24] Y. Liu, W. Wang, A. Wang, Adsorption of lead ions from aqueous solution by using carboxymethyl cellulose-*g*-poly (acrylic acid)/attapulgite hydrogel composites, Desalination 259 (2010) 258–264.
[25] J. Wang, X. Lin, X. Luo, Y. Long, A sorbent of carboxymethyl cellulose loaded with zirconium for the removal of fluoride from aqueous solution, Chem. Eng. J. 252 (2014) 415–422.
[26] A. Hiroki, H.T. Tran, N. Nagasawa, T. Yagi, M. Tamada, Metal adsorption of carboxymethyl cellulose/carboxymethyl chitosan blend hydrogels prepared by Gamma irradiation, Radiat. Phys. Chem. 78 (2009) 1076–1080.
[27] L. Qiu, Z. Shao, P. Xiang, D. Wang, Z. Zhou, F. Wang, W. Wang, J. Wang, Study on novel functional materials carboxymethyl cellulose lithium (CMC-Li) improve high-performance lithium-ion battery, Carbohydr. Polym. 110 (2014) 121–127.
[28] Z. Zhang, Y. Yan, Y. Chen, L. Zhang, Investigation of CO_2 absorption in methyldiethanolamine and 2-(1-piperazinyl)-ethylamine using hollow fiber membrane contactors: Part C. Effect of operating variables, J. Nat. Gas Sci. Eng. 20 (2014) 58–66.
[29] S. Chen, W. Shen, F. Yu, W. Hu, H. Wang, Preparation of amidoximated bacterial cellulose and its adsorption mechanism for Cu^{2+} and Pb^{2+}, J. Appl. Polym. Sci. 117 (2010) 8–15.
[30] S. Deng, R. Bai, J.P. Chen, Aminated polyacrylonitrile fibers for lead and copper removal, Langmuir 19 (2003) 5058–5064.
[31] X. Yang, J. Li, T. Wen, X. Ren, Y. Huang, X. Wang, Adsorption of naphthalene and its derivatives on magnetic graphene composites and the mechanism investigation, Colloids Surf., A 422 (2013) 118–125.
[32] S. Zhang, M. Zeng, J. Li, J. Li, J. Xu, X. Wang, Porous magnetic carbon sheets from biomass as an adsorbent for the fast removal of organic pollutants from aqueous solution, J. Mater. Chem. 2 (2014) 4391–4397.
[33] S. Zhang, W. Xu, M. Zeng, J. Li, J. Li, J. Xu, X. Wang, Superior adsorption capacity of hierarchical iron oxide@magnesium silicate magnetic nanorods for fast removal of organic pollutants from aqueous solution, J. Mater. Chem. 1 (2013) 11691–11697.
[34] G. Giakisikli, A.N. Anthemidis, Magnetic materials as sorbents for metal/metalloid preconcentration and/or separation. A review, Anal. Chim. Acta 789 (2013) 1–16.
[35] W. Xie, J. Wang, Immobilized lipase on magnetic chitosan microspheres for transesterification of soybean oil, Biomass Bioenergy 36 (2012) 373–380.
[36] Q. Peng, Y. Liu, G. Zeng, W. Xu, C. Yang, J. Zhang, Biosorption of copper(II) by immobilizing *Saccharomyces cerevisiae* on the surface of chitosan-coated magnetic nanoparticles from aqueous solution, J. Hazard. Mater. 177 (2010) 676–682.
[37] T.G. Yan, L.J. Wang, Adsorption of C.I. Reactive Red 228 and Congo Red dye from aqueous solution by amino-functionalized Fe 3 O 4 particles: Kinetics, equilibrium, and thermodynamics, Water Sci. Technol. 69 (2014) 612–621.
[38] P. Senthil Kumar, S. Ramalingam, C. Senthamarai, M. Niranjanaa, P. Vijayalakshmi, S. Sivanesan, Adsorption of dye from aqueous solution by cashew nut shell: Studies on equilibrium isotherm, kinetics and thermodynamics of interactions, Desalination 261 (2010) 52–60.
[39] M. Ghaedi, A. Hassanzadeh, S.N. Kokhdan, Multi-walled carbon nanotubes as adsorbents for the kinetic and equilibrium study of the removal of Alizarin Red S and Morin, J. Chem. Eng. Data 56 (2011) 2511–2520.
[40] Y.S. Ho, G. McKay, A comparison of chemisorption kinetic models applied to pollutant removal on various sorbents, Process Saf. Environ. Prot. 76 (1998) 332–340.
[41] Y.S. Ho, G. McKay, Pseudo-second order model for sorption processes, Process Biochem. 34 (1999) 451–465.
[42] G. Bayramoglu, B. Altintas, M.Y. Arica, Adsorption kinetics and thermodynamic parameters of cationic dyes from aqueous solutions by using a new strong cation-exchange resin, Chem. Eng. J. 152 (2009) 339–346.
[43] W. Weber, J. Morris, Kinetics of adsorption on carbon from solution, J. Sanit. Eng. Div. Am. Soc. Civ. Eng. 89 (1963) 31–60.
[44] G. Crini, F. Gimbert, C. Robert, B. Martel, O. Adam, N. Morin-Crini, F. De Giorgi, P.M. Badot, The removal of Basic Blue 3 from aqueous solutions by chitosan-based adsorbent: Batch studies, J. Hazard. Mater. 153 (2008) 96–106.
[45] G.E. Boyd, A.W. Adamson, L.S. Myers, The exchange adsorption of ions from aqueous solutions by organic zeolites. II. Kinetics 1, J. Am. Chem. Soc. 69 (1947) 2836–2848.
[46] V. Vimonses, S. Lei, B. Jin, C.W.K. Chow, C. Saint, Adsorption of congo red by three Australian kaolins, Appl. Clay Sci. 43 (2009) 465–472.
[47] L. Zhou, J. Jin, Z. Liu, X. Liang, C. Shang, Adsorption of acid dyes from aqueous solutions by the ethylenediamine-modified magnetic chitosan nanoparticles, J. Hazard. Mater. 185 (2011) 1045–1052.
[48] A.H. Chen, S.M. Chen, Biosorption of azo dyes from aqueous solution by glutaraldehyde-crosslinked chitosans, J. Hazard. Mater. 172 (2009) 1111–1121.
[49] A.H. Chen, S.C. Liu, C.Y. Chen, C.Y. Chen, Comparative adsorption of Cu(II), Zn(II), and Pb(II) ions in aqueous solution on the crosslinked chitosan with epichlorohydrin, J. Hazard. Mater. 154 (2008) 184–191.
[50] J. Tellinghuisen, Van't Hoff analysis of K°(T): How good…or bad?, Biophys. Chem. 120 (2006) 114–120.